A vector sensing scheme for underwater acoustics based on particle velocity measurements

Unnikrishnan Kuttan Chandrika, Vishnu N. Hari
Acoustic Research Laboratory
National University of Singapore, Singapore

***Abstract*—We present a particle velocity sensing scheme for underwater acoustic vector sensors, which utilizes a nature-inspired bionic hair based transduction scheme. The hair based sensor offers an attractive option for particle velocity sensing with low sensor size, but it is limited by low sensitivity. This limitation can be overcome by using an acoustic horn for amplification, and using a sensitive measurement system such as a fibre optic system. We undertake simulation studies to evaluate the feasibility of the vector sensing scheme. For the small sensor sizes and low frequencies considered, the effects of viscosity become dominant. We discuss the effects of viscosity through parameteric studies and its effect on determining the operating parameters of the sensing scheme.**

I. Introduction

Acoustic vector sensors (AVS) are sensors that measure the acoustic pressure as well as the components of acoustic particle velocity at a point. AVS technology has grown rapidly in recent years due to the established superiority of AVS over pressure sensors in signal processing applications. A single point measurement using a conventional hydrophone yields only the scalar information on the sound field, viz. the pressure amplitude. On the other hand, the particle velocity measurements in an AVS provide additional information about the acoustic field, the direction of the impinging acoustic waves, which is not available in the case of a single hydrophone [1]. This gives the AVS many advantages over hydrophones such as compactness, better and unambiguous localisation for underwater acoustic sensing applications and flexibility of sensor spacing. Several experimental setups such as the DIFAR array [2] and Makai experiments [3] have demonstrated the effectiveness of AVS. AVS have been shown to be effective in signal detection [4], direction-of-arrival estimation [5], communication [6], imaging [7] and seabed characterization [8].

Vector sensing requires direct measurement of pressure gradient or particle motion. Quantities like particle displacement, particle velocity and particle acceleration contain amplitude and directionality information about the sound field. There have been many attempts on the measurement of all the above quantities. Early works in AVS technology focused on estimation of the direction of the sound field from pressure gradient measurements [9], which suffered from finite difference and phase mismatch errors [10]. Hot wire anemometry has been extensively used for flow measurements [11], but it has not been effectively adapted for underwater applications due to loss in sensitivity when used in impedance matching fluids like castor oil [12]. Most underwater acoustic particle velocity measurement schemes exploit the principle that the motion of a freely floating neutrally buoyant sphere placed in a sound field follows the particle velocity of the water [13]. The arrival of highly sensitive piezo-ceramic material like PMN-PT with better sensitivity than conventional PZT, has created interest in accelerometer based AVS for underwater applications [10]. But the performance of these sensors suffer from relatively high noise floor compared to ambient noise conditions in the ocean. Moreover, the direct measurement of particle velocity has some advantages from the operational point of view, especially for acoustic particle motion based sensing, because the particle velocity is directly proportional to the pressure amplitudes.

Particle velocity sensing using bionic hair sensors has generated significant interest in recent years [14]. Bionic hair sensors can be adapted for AVS with huge benefits in terms of sensor size as demonstrated by Zhang et. al. [15]. The main challenge is that the particle velocity sensors are relatively less sensitive compared to hydrophones and usually suffer from higher noise floor. In order to deal with the problem of low sensitivity, we investigate the effect of using horns in order to amplify the particle velocities measured. Recent simulation and experimental works show that horns can be used as particle velocity amplifiers with a uniform frequency response over a wide frequency range [16]. Hence it is possible to apply these particle velocity amplifiers to mitigate the effect of the inherent high noise floor reported in many hair based velocity sensing schemes.

Even with the application of acoustic horns, the particle velocities corresponding to ambient noise levels in the ocean are very low. Hence a high sensitivity transduction scheme is needed to achieve reliable measurements down to ambient noise levels. Fibre optic sensing technology is an ideal candidate for high-performance underwater acoustic sensing applications due to its many benefits like remote sensing, ease of multiplexing and improved reliability due to the absence of wet-end electronics [17]. Fibre laser based accelerometers mounted in a neutrally buoyant sphere have been used previously as well to measure the acoustic particle velocity [18], [19].

We propose to use an interferometric sensing scheme that employs a fibre laser mounted on a cantilever transducer to realise a compact high-performance vector sensor. The transducer is placed inside an acoustic horn for particle velocity amplification. When low frequencies and small sensor sizes are considered, the effect of viscosity on the acoustic field becomes predominant. We discuss the effect of viscosity in the transduction scheme and its impacts on the operating range of the sensor, which has not been considered in any previous work. We undertake simulation studies to understand the trade-offs in the system due to viscosity effects, and

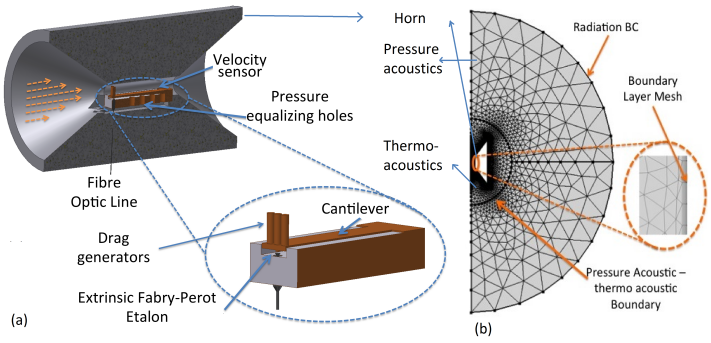

Fig. 1: (a) Sensing setup with fibre laser mounted on a cantilever to act as particle velocity sensor (b) Axis-symmetric finite-element model for analysis of the setup.

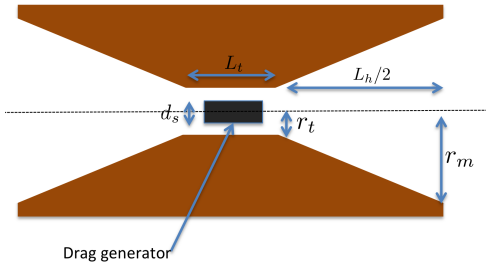

Fig. 2: Configuration with important parameters considered in the analysis

investigate the variation in particle velocity amplification with various parameters of the horn. Thereby, we arrive at a suitable sensor configuration for good performance within the desired operating range.

The paper is organized as follows. In section II, we discuss the theory that governs the particle velocity field, and its amplification in a horn. In section III, we investigate via finite-element analysis, the effect of viscosity when using the acoustic horns for amplification, and the trade-offs introduced into the sensor design due to viscosity effects. In section IV we discuss the transduction and sensing scheme using a fibre laser mounted on a bionic hair-based setup, and in section V, we conclude the paper.

II. Theory

A. Wave equation

The complex envelope of the acoustic particle velocity (u_{ac}) due to propagation of an acoustic plane wave is given in equation (1) where P is the complex envelope of the pressure, ρ is the density and c is the sound speed of the medium.

$$u_{ac} = \frac{P}{\rho c} \tag{1}$$

Consider a sensing configuration where the particles in the fluid move with a velocity u_{ac} and a body which acts as the sensor moves with a velocity u_s. The force experienced by the body has three components; viz. the buoyancy force experienced due to fluid acceleration, inertia force arising from the added mass, and the drag force experienced by the body. The drag force has a direct dependence on the fluid velocity and is in phase with the velocity while the inertia and buoyancy forces are in phase with acoustic particle acceleration. The drag force experienced by a sphere oscillating in a stationary viscous fluid can be written as

$$F_d(f) = -6\pi a\mu \left[\left(1 + \frac{a}{\delta(f)}\right) + j\frac{a}{\delta(f)}\left(1 + \frac{2a}{9\delta(f)}\right)\right] u_s \tag{2}$$

where δ, the thickness of the viscous boundary layer or Stokes layer, is given as [20]

$$\delta(f) = \sqrt{\frac{\mu}{\rho\pi f}}. \tag{3}$$

In equation (2) and (3), a is the radius of the sphere, μ is the dynamic viscosity of the fluid and f is the frequency. The drag force term given in equation (2) contains the forces due to viscous drag as well as inertia forces due to added mass effects. When the motion of the body is excited by oscillating fluid, in addition to the drag force, the buoyancy forces from the fluid should be added and relative velocity should be used in place of u_s. The second term in the square brackets on the right side of equation (2) becomes predominant with increase in frequency as the boundary layer thickness has an inverse relationship with frequency. The buoyancy force which is proportional to fluid acceleration also increases with increase in frequency. But at low frequencies the viscous force, represented by first term in the square brackets on the right side of equation (2) is the dominant contributor to total force experienced by the body.

The unsteady Reynolds number (R_{ac}) defined in equation (4) can be used to differentiate the predominant effect in drag force experienced by the body due to an oscillating flow. For a sphere excited by an oscillating flow, the viscous effects are predominant when $R_{ac} < 1$.

$$R_{ac} = \frac{2\pi\rho f a^2}{\mu} \tag{4}$$

B. Acoustic Horns

The performance of acoustic sensors can be improved by use of acoustic horns which lend an improvement due to increased directivity. We propose the configuration depicted in Fig. 1(a) to establish the feasibility of vector sensing which utilises acoustic horns for particle velocity amplification. The transducer consisting of a cantilever setup is at the center of an open-ended horn. Viscous effects become important as the size of the sensor configuration reduces. Many practical horn acoustic systems utilize Webster horn equations [21] in performance predictions. But key assumptions used in its derivation such as absence of viscosity and uniform distribution of energy across the wavefront, invalidate it for the current application. Finite element analysis technique is employed by us to simulate the effect of horns on the performance of the acoustic sensor. Figure 1(b) shows an axisymmetric finite element model used to simulate the sound propagation through horns using the software COMSOL. A schematic showing the dimensional parameters of the horn is shown in Fig. 2. We define the length ratio $R_L = \frac{L_h}{r_t}$ and radius ratio $R_r = \frac{r_m}{r_t}$, where L_h refers to horn length, and r_t and r_m refer to radius of throat and mouth of the horn respectively.

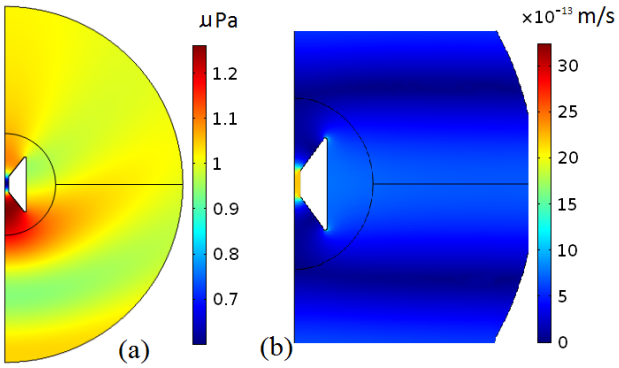

Fig. 3: (a) RMS pressure and (b) particle velocity distribution in horn for a plane wave. RMS particle velocity of plane wave in water with 1 μPa RMS amplitude is 6.67×10^{-13} m/s

Since we focus on viscous effects in our current study, the traditional wave equation needs to be modified to include the effect of viscosity. As the particle velocities are very small, the velocity convection terms in the Navier-Stokes equation can be neglected to simplify the governing equations. These equations can be further simplified by performing the analysis in the frequency domain. Hence, the continuity and momentum balance given in equations (5) and (6) are solved in COMSOL in the vicinity of the sensor, marked as thermo-acoustic domain in Fig. 1(b). As the effect of viscosity is negligible further away from the sensor configuration, the conventional wave-equation is employed in this region, marked as pressure-acoustic domain in Fig. 1(b). In equations (5) and (6), ρ_0 is the background density, p', $\mathbf{u}'$, and ρ' represent fluctuations in pressure, velocity and density over their background values. A boundary layer region exists due to viscosity of the fluid. Meshing of the boundary layer with sufficient resolution is essential in the current finite-element analysis.

$$i\omega\rho' = -\rho_0(\Delta.\mathbf{u}') \tag{5}$$

$$i\omega\rho_0\mathbf{u}' = \Delta.\left(\mu\left(\Delta\mathbf{u}' + (\Delta\mathbf{u}')^T\right) - p'\mathbf{I} - (\mu_B - \frac{2\mu}{3})(\Delta.\mathbf{u}')\mathbf{I}\right) \tag{6}$$

TABLE I: Parameters used in the analysis

Feature	Value
Throat radius r_t	2.5 mm
Length of Throat L_t	20 mm
Radius ratio R_r	5
Length ratio R_L	10
Fluid medium	water

Figure 3(a) shows the pressure distribution for a plane wave at 10 kHz with 1 μPa root-mean-square (RMS) amplitude propagating along the axis of the horn, and Fig. 3(b) plots the corresponding particle velocity distribution, for a configuration showed in Fig. 1(a). The dimensions of the horn are as specified in table I. It can be observed that at the frequency considered, which is much lower than the acoustic resonance of the horn, the axial variation of pressure in the horn (Fig. 3(a)) is negligible. But there is a significant amplification of particle velocity at the throat of the horn, which reduces in the axial direction as one moves outward from the throat towards the mouth and exterior of the horn (Fig. 3(b)). This might appear counter intuitive with reference to acoustic pressure horns used in electro-acoustic speakers. But the analysed configuration has an open throat unlike acoustic pressure horns, where the throat is blocked by a high impedance electro-acoustic device.

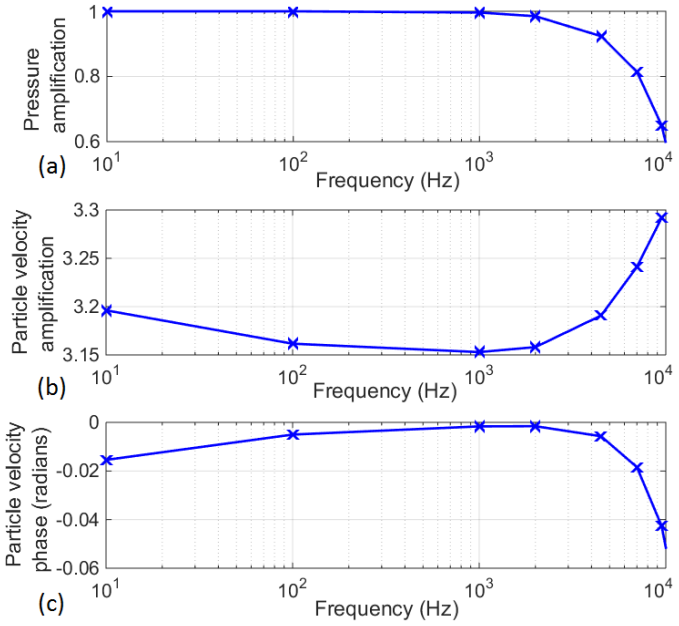

Fig. 4: Variation in (a) acoustic pressure amplification, (b) particle velocity amplification and (c) phase of the particle velocity at throat of the horn, with frequency.

The frequency response of the acoustic field measurements in the horn over a frequency range of interest was computed. Figure 4 shows the variation of (a) pressure amplification and (b) particle velocity amplification with frequency at the throat of the horn. We see that the analysed horn configuration can provide uniform amplification in particle velocity over a wide frequency range. Figure 4(c) shows the variation in phase of the particle velocity at the throat of the horn with the frequency. It can be noted that the phase change is minimal and smooth. Hence, the particle velocity at the throat of the horn exhibits a frequency response favorable to sensing.

III. Simulation Study

A. *Effect of viscosity*

Viscosity plays a major role in the proposed sensing scheme. The effect of viscosity becomes more pronounced as the horn dimensions reduce. Viscosity effects are predominant in the region closer to the wall called Stokes layer. In the outer region an inviscid core is formed. The order of magnitude of thickness δ of the Stokes layer is given in (3). Note that the Stokes layer thickness has a direct dependence on viscosity and its thickness reduces with increase in frequency.

We undertake further simulations to understand the effect of viscosity on the particle velocity amplification by horns. The

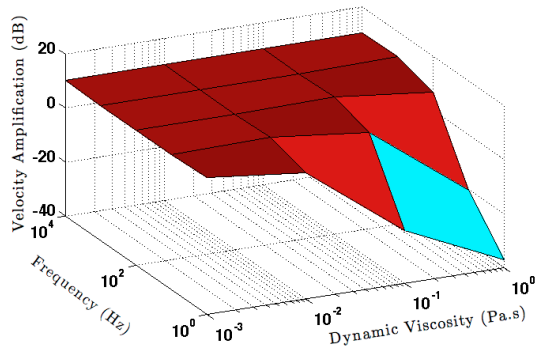

Fig. 5: Variation of velocity amplification (dB) at throat of the horn with frequency and dynamic viscosity

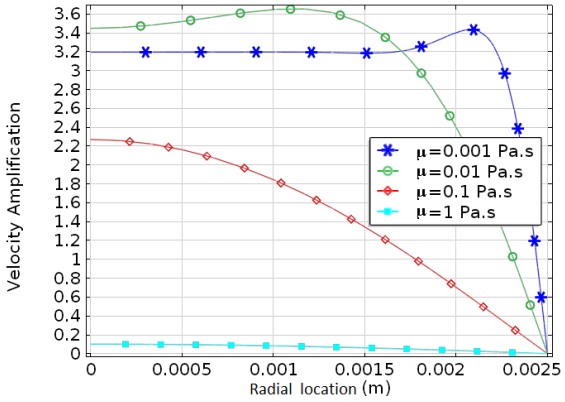

Fig. 6: Variation of velocity amplification at throat of the horn with radial distance at different values of dynamic viscosity μ

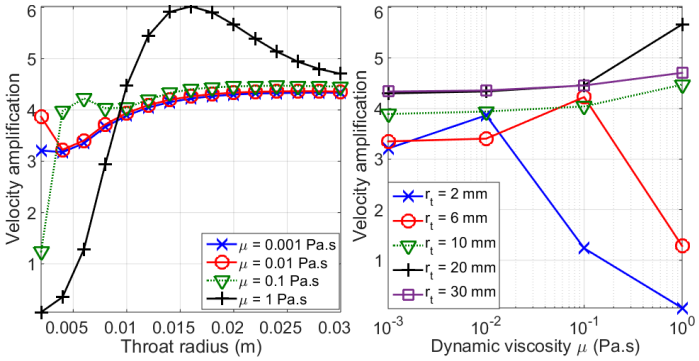

Fig. 7: Variation of particle velocity amplification with (a) throat radius r_t at different values of dynamic viscosity μ, and (b) dynamic viscosity μ for different values of r_t

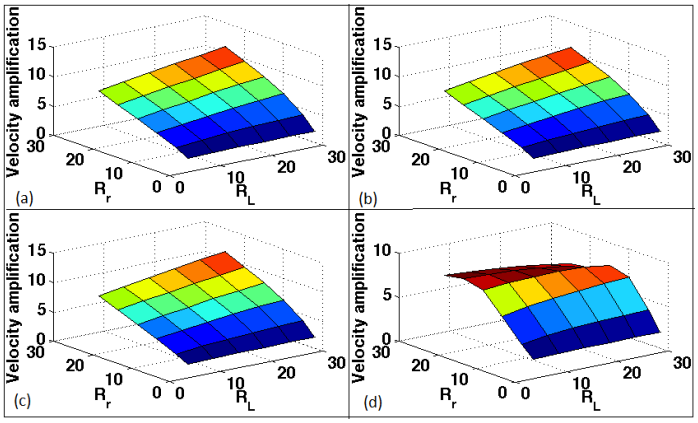

Fig. 8: Variation of particle velocity amplification with R_r and R_L for frequency f = (a) 10 Hz (b) 100 Hz, (c) 1000 Hz, (d) 10000 Hz

value of dynamic viscosity was varied from 0.001 to 1 Pa.s, which covers a range of fluids from water to castor oil. Figure 5 shows the variation of acoustic particle velocity amplification at the throat of the horn with frequency and dynamic viscosity, with the horn dimensional parameters as specified in table I. Although the effect of viscosity is negligible at very high frequencies, the acoustic particle velocity amplification reduces significantly at low frequencies for the analysed configuration. This arises due to the fact that the thickness of the viscous layer increases with viscosity.

Figure 6 shows the radial profile of the acoustic particle velocity amplification at the throat section of the horn at different values of dynamic viscosity using the parameters described in table I, for a plane wave of frequency 10 Hz. The maximum particle velocity occurs beyond the central inviscid core where the velocity is uniform (eg. at a radial distance of 2.1 mm for $\mu = 0.001$). At low frequencies or high viscosities, the effect of viscosity dominates the entire throat section and significantly reduces the particle velocity at the throat. For example, Fig. 6 shows that at 10 Hz, an acoustic horn with a throat diameter of 5 mm filled with castor oil will result in particle velocity reduction rather than amplification.

Figure 7 plots the variation of the particle velocity amplification with (a) horn throat radius r_t for a range of values of μ, and (b) with μ for a range of values of r_t. The frequency of the plane wave is assumed to be 10 Hz. Figure 7 makes it clear that for good amplification by the horn, diameter of the horn should be sufficiently large as the viscosity increases. For example, application of castor oil ($\mu = 1$) requires a minimum throat diameter of the order of 10 mm at low frequencies (of the order of 10 Hz) for good amplification.

From Figs. 5-7, we see that for designing the sensing system, the effect of viscosity forces us to make a trade-off between the dynamic viscosity μ of the fluid, size of the horn (dependent on throat radius r_t) and the sensing performance at low frequencies. This trade-off affects the low frequency operating range.

We now undertake a parametric study to investigate the variation in particle velocity amplification with the dimensional ratios R_r and R_L. The throat radius is fixed at 2.5 mm and material properties of water are used in the simulation. Figure 8 shows the results from the parametric study. It can be observed that in general, the velocity amplification increases with both R_L and R_r. The amplification is independent of R_L at low R_r values. But as R_r increases, increase in R_L also provides additional amplification. We also observe that at very high

frequencies there is a deviation in the velocity amplification trend. This arises due to the fact that as R_r increases, the horn dimensions are comparable to the acoustic wavelengths. Hence the acoustic modes of the horns could be contributing to this observed behaviour. This discussion outlines another trade-off to be tackled while choosing the operating range of the horn-based sensor, which is that of sensor size (determined by R_r and R_L) against velocity amplification of the horn and the high frequency operating limit.

B. Directivity

A 3D acoustic analysis was carried out to study the directivity pattern from the acoustic horn. The direction of the plane wave was varied to study the directivity pattern of the horn. Figure 9 shows the directivity pattern (velocity amplification plotted against direction of the plane wave) for a horn with dimensions given in table I for frequencies 100 Hz, 1000 Hz and 10000 Hz.

IV. Transduction and Sensing

A. Transduction scheme

TABLE II: Parameters used in the analysis

Feature	Value
Throat radius r_t	4.5 mm
Length of Throat L_t	20 mm
Cylinder radius	1.25 mm
Radius ratio R_r	7.2
Length ratio R_L	14.4
Density of fluid	1000 kg/m^3
Speed of sound	1480 m/s
Dynamic Viscosity	(0.001, 0.01, 0.1,1) Pa.s

While horns can act as particle velocity amplifiers, we are interested in the development of a suitable transduction scheme which can sense the particle velocity at the throat of the horn. As explained in section II, a transduction mechanism which can sense the viscous drag forces can give direct measurement of particle velocity at the throat of the horn. To understand the performance of such a transduction scheme, a concentric cylinder which acts as a drag generator was placed at axis of the horn in the throat area in the analysed model. The shear stress τ acting on the cylinder can be calculated from the velocity gradient as

$$\tau = \mu \frac{du}{dr} \tag{7}$$

where μ is the dynamic viscosity, u is the axial velocity and r is the radial displacement. The shear stress calculated from equation (7) can be integrated over the cylinder surface to estimate the skin friction drag force F_{drag}. The basic assumptions used here are that the motion of the drag generating cylinder is negligible in comparison to particle velocity and the cylinder dimensions are small compared to the wavelength of the acoustic wave. The cylinder radius is considered to be equal to 0.8 times the horn throat radius. Figure 10 plots the variation in drag force with frequency for different values of μ for the parameters given in table II. A wave of 1 Pa is assumed to be incident on the sensor. We see that using castor oil ($\mu = 1$) yields the highest drag force for the setup.

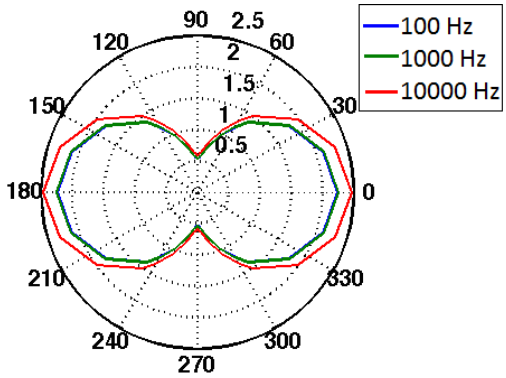

Fig. 9: Directivity pattern for the horn with dimensional parameters given in table I

B. Optical measurement scheme

Acoustic particle velocity sensing is very challenging, especially in an underwater scenario due to the very high acoustic impedance of water. As estimated in the previous section, the viscous drag force levels experienced by a drag generator is only of the order of picoNewtons for sea state zero ambient noise conditions. Although challenging, the optical sensing techniques can achieve such fine measurement resolutions. A setup consisting of fibre lasers mounted on a suitable cantilever or set of cantilevers is one such plausible measurement technique.

Fibre lasers are Fabry-Perot resonance cavities created on an active fibre (rare earth element doped fibre) by writing spectrally matched Bragg gratings. They absorb the light energy from an external pump source and generate laser at wavelengths which depend on the grating pitch, effective refractive index of the resonance cavity and emission bandwidth of the dopant used in the fibre. Changes in the grating structure due to strain or temperature results in corresponding changes in the fibre laser output wavelength. Multiple fibre lasers can be connected on a single optical fibre line using wavelength division multiplexing scheme through careful design of grating structure of individual fibre lasers. Interferometric systems along with phase demodulators are usually employed to convert the fibre laser wavelength changes into electrical signals. A detailed review of the operating principles of a fibre laser sensors and associated interferometric techniques can be found in [22] and [17].

Figure 11 shows a feasible sensing configuration based on cantilever structure. The application of cantilever in sensing provides us with the flexibility to select the dimensional parameters of the cantilever to achieve required performance characteristics of the sensor system. The fibre laser is mounted on the bottom side of the cantilever and the drag generating cylinder on the top side as shown in Fig. 11. The drag generating cylinder is offset from the cantilever to generate bending moment which results in strain on the fibre. Consider an acoustic horn used in conjunction with a cantilever config-

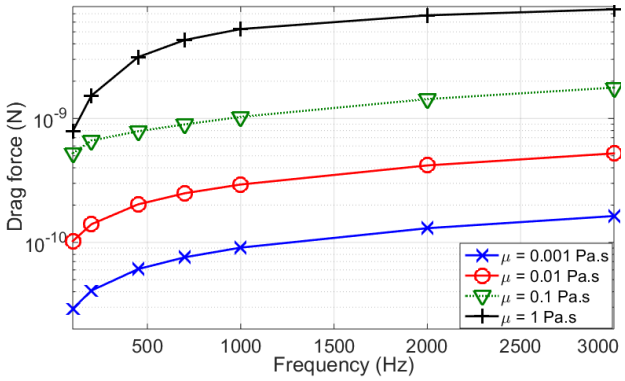

Fig. 10: Skin friction drag on the cylinder due to an incident plane wave for different values of dynamic viscosity μ

uration. The strain acting on the fibre can be calculated as

$$\varepsilon = \frac{My_f}{EI} \tag{8}$$

where $M = F_{drag} \times y_s$ is the bending moment at an offset y_s, E is the elastic modulus and I the area moment of inertia of the beam cross section.

The phase resolution and noise floor characteristics of the fibre laser hydrophone system depend directly on three major parameters: measurement resolution of the opto-electronic instrumentation, inherent frequency noise of the fibre laser and the optical path imbalance used in the interferometer [17]. Commercial phase demodulation systems that can achieve measurement resolutions of the order of a few micro radians are available off the shelf.

C. Sensitivity of the overall system

Based on our understanding from the discussions in sections III-A, IV-A and IV-B, we can choose suitable parameters for the sensing system that yield desirable characteristics within the operating range chosen. As an example, we consider a particle velocity sensor with specifications similar to a commercially available vector sensor from Microfine Materials Technologies [23]. The velocity sensor is designed to work in the frequency range 100 Hz to 3000 Hz. The medium is chosen as castor oil ($\mu = 1$ Pa.s) to maximize the drag force on the drag-generating cylinder. For this medium, we find that the throat radius must be atleast 4.5 mm in order to achieve nearly uniform amplification by the horn over all frequencies and avoid the effects of the viscous layer. R_r and R_L are chosen as 7.2 and 14.4 respectively, so we obtain a horn with diameter and length of 65 mm. Thus, we obtain the dimensional parameters given in table II.

For transduction, a cylinder with radius equal to 0.8 times the throat radius is considered. Consider the T-section setup given in Fig. 11 with a beam section with a Young's modulus of 10 GPa. At a frequency of 1000 Hz, a strain output on the order of 10^{-11} can be achieved at an offset of 5 mm for an incident wave of 1 Pa, using a drag force value of 7×10^{-9} N as observed in Fig.10. This sensitivity figure could be

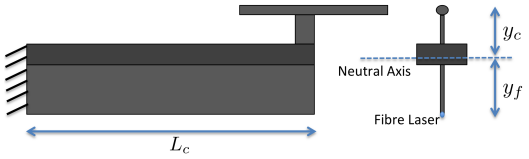

Fig. 11: Fibre laser mounted on a cantilever to act as particle velocity sensor

improved by optimising the design of cantilever structure and drag generators.

Fibre laser hydrophones have been shown to be able to detect strains of 8×10^{-15} at 1000 Hz [24]. From this, we can compute that the minimum particle velocity level detectable by the system is 55 dB re 6.67×10^{-13} m/s. This level is quite small, and is an order of magnitude more than sea state zero ambient noise conditions. Hence, the simple example considered by us demonstrates the effectiveness of the sensor setup. Further improvements to the system are possible by optimizing the parameters of the T-section and horn dimensional parameters.

V. Conclusions

We explored a method of acoustic vector sensing using bionic hair sensors for transducing acoustic particle velocity. This method can provide gains in terms of sensor size over other methods. One of the challenges faced in this technique is its low sensitivity. This problem can be overcome by using an acoustic horn to amplify the particle velocity sensed, and a highly sensitive laser-interferometric sensing system to pick up the transduced strain output from the sensor.

The acoustic horn provides good amplification in particle velocity that is uniform over a wide frequency range, with minimal phase distortion. The effect of viscosity imposes some limitations to the operating range and performance of the horn due to the thickness of the viscous layer. The dimensions of the horn and the fluid medium used, determine the operating frequency range and amplification. By suitably choosing the horn parameters, it is possible to obtain the good performance within the low frequency and high frequency operating limits.

The transducer, a hair-based cantilever system, is placed at the center of the throat of the horn. If a laser-interferometric sensing system is used, we show that it is possible to achieve a measurable output from the cantilever-based transducer which is within the sensing threshold of the laser interferometer. Thus we have demonstrated the good sensing capabilities of the proposed sensing configuration

References

[1] A. Nehorai and E. Paldi, "Acoustic vector-sensor array processing," *IEEE Transactions on Signal Processing*, vol. 42, no. 9, pp. 2481–2491, 1994.

[2] G. D'Spain, W. Hodgkiss, G. Edmonds, J. Nickles, F. Fisher, and R. Harriss, "Initial Analysis Of The Data From The Vertical DIFAR Array," in *OCEANS 92*, vol. 1. Newport, Rhode Island: IEEE, 1992, pp. 346–351.

[3] M. Porter, B. Abraham, M. Badiey, M. Buckingham, T. Folegot, P. Hursky, S. Jesus, K. Kim, B. Kraft, V. McDonald, C. DeMoustier, J. Presig, S. Roy, M. Siderius, H. Song, and W. Yang, "The Makai experiment: High frequency acoustics," in *8th ECUA*, S. Jesus and O. C. Rodríguez, Eds., Carvoerio, Portugal, 2006, pp. 9–18.

[4] V. Hari, G. Anand, and A. Premkumar, "Narrowband signal detection techniques in shallow ocean by acoustic vector sensor array," *Digital Signal Processing*, vol. 23, no. 5, pp. 1645–1661, Sep. 2013.

[5] M. Hawkes and A. Nehorai, "Acoustic vector-sensor beamforming and Capon direction estimation," *IEEE Transactions on Signal Processing*, vol. 46, no. 9, pp. 2291–2304, 1998.

[6] C. Chen and A. Abdi, "A vector sensor receiver for chirp modulation in underwater acoustic particle velocity channels," in *Proceedings of Conference on Underwater communications: Channel modelling and validation*, Sestri Levante, 2012, pp. 1–8.

[7] D. Lindwall, "Imaging marine geophysical environments with vector acoustics," *The Journal of the Acoustical Society of America*, vol. 120, no. 3, p. EL43, 2006.

[8] P. Santos, O. Rodríguez, P. Felisberto, and S. Jesus, "Seabed geoacoustic characterization with a vector sensor array." *The Journal of the Acoustical Society of America*, vol. 128, no. 5, pp. 2652–63, Nov. 2010.

[9] T. Schultz, "Acoustic wattmeter," *The Journal of the Acoustical Society of America*, vol. 28, no. 4, pp. 693–699, 1956.

[10] K. Kim, T. Gabrielson, and G. Lauchle, "Development of an accelerometer-based underwater acoustic intensity sensor," *The Journal of the Acoustical Society of America*, vol. 116, no. 6, pp. 3384–3392, 2004.

[11] H.-E. De Bree, "The microflown: An acoustic particle velocity sensor," *Acoustics Australia*, vol. 31, no. 3, pp. 91–94, 2003.

[12] M. Hezemans, "Feasibility study to adapt the microflown vector sensor for underwater use," Master's thesis, Monterey, California. Naval Postgraduate School, 2012.

[13] C. Leslie, J. Kendall, and J. Jones, "Hydrophone for measuring particle velocity," *The Journal of the Acoustical Society of America*, vol. 28, no. 4, pp. 711–715, 1956.

[14] J. Tao and X. Yu, "Hair flow sensors: from bio-inspiration to bio-mimicking - a review," *Smart Materials and Structures*, vol. 21, no. 11, p. 113001, 2012.

[15] B. Zhang, H. Qiao, S. Chen, J. Liu, W. Zhang, J. Xiong, C. Xue, and G. Zhang, "Modeling and characterization of a micromachined artificial hair cell vector hydrophone," *Microsystem Technologies*, vol. 14, no. 6, pp. 821–828, 2008.

[16] D. Donskoy and B. Cray, "Horns as particle velocity amplifiers," *The Journal of the Acoustical Society of America*, vol. 130, no. 5, pp. EL311–EL315, 2011.

[17] C. Kirkendall and A. Dandridge, "Overview of high performance fibre-optic sensing," *Journal of Physics D: Applied Physics*, vol. 37, no. 18, p. R197, 2004.

[18] P. Jackson, S. Foster, and S. Goodman, "A fibre laser acoustic vector sensor," in *20th International Conference on Optical Fibre Sensors*. International Society for Optics and Photonics, 2009, pp. 750 329–750 329.

[19] W. Zhang, F. Zhang, R. Ma, J. He, F. Li, and Y. Liu, "Fiber laser vector hydrophone: theory and experiment," in *21st International Conference on Optical Fibre Sensors (OFS21)*. International Society for Optics and Photonics, 2011, pp. 77 533D–77 533D.

[20] S. van Netten, "Hydrodynamic detection by cupulae in a lateral line canal: functional relations between physics and physiology," *Biological cybernetics*, vol. 94, no. 1, pp. 67–85, 2006.

[21] A. G. Webster, "Acoustical impedance and the theory of horns and of the phonograph," *Proceedings of the National Academy of Sciences of the United States of America*, vol. 5, no. 7, p. 275, 1919.

[22] D. Hill, P. Nash, D. Jackson, D. Webb, S. O'Neill, I. Bennion, and L. Zhang, "Fiber laser hydrophone array," in *Proceedings of SPIE on Fiber Optic Sensor Technology and Applications*, vol. 3860, Boston, USA, 1999, p. 55.

[23] (2015, Jun.) Accelerometer-based acoustic vector sensor. [Online]. Available: http://www.microfine-piezo.com/files/1399104906434.pdf

[24] S. Foster, A. Tikhomirov, and J. Harrison, "Fundamental limits on low frequency cavity fluctuations in optical fibre lasers," in *Quantum Electronics Conference Lasers and Electro-Optics (CLEO/IQEC/PACIFIC RIM), 2011*, Aug 2011, pp. 1193–1195.